




Reductive Coupling Synthesis of a Soluble Poly(9,10-anthrylene ethynylene)

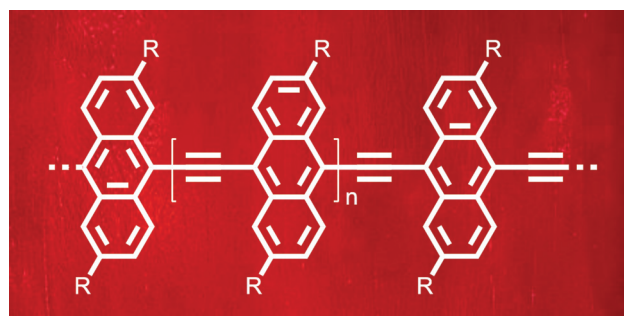
Isabell Geisler^aMichael Forster^aBujamin Misimi^bJakob Schedlbauer^c Thomas Riedl^b John M. Lupton^c Ullrich Scherf^a 

^a Bergische Universität Wuppertal, Macromolecular Chemistry Group (buwmakro) and Wuppertal Center for Smart Materials & Systems, Gauss-Str. 20, D-42119, Wuppertal, Germany


^b Bergische Universität Wuppertal, Chair of Electronic Devices and Wuppertal Center for Smart Materials & Systems, Rainer-Gruentner-Str. 21, D-42119 Wuppertal, Germany

^c Universität Regensburg, Institut für Experimentelle und Angewandte Physik, Universitätsstrasse 31, D-93053 Regensburg, Germany
scherf@uni-wuppertal.de

Dedicated to Professor Peter Bäuerle on the occasion of his 65th birthday.



Received: 13.01.2021
Accepted after revision: 17.03.2021
DOI: 10.1055/a-1472-6806; Art ID: om-21-0003oa

License terms: 

© 2021. The Author(s). This is an open access article published by Thieme under the terms of the Creative Commons Attribution License, permitting unrestricted use, distribution, and reproduction so long as the original work is properly cited. (<https://creativecommons.org/licenses/by/4.0/>)

Abstract A fully soluble poly(9,10-anthrylene ethynylene), poly[2,6-(2-octyldecyl)-9,10-anthrylene ethynylene] **PAAE**, with moderate degrees of polymerization P_n of ca. 10 is generated in a reductive, dehalogenative homocoupling scheme, starting from a 2,6-dialkylated 9,10-bis(dibromomethylene)-9,10-dihydroanthracene monomer and n -BuLi/CuCN as the reducing agent. **PAAE** shows surprisingly broad and unstructured absorption and photoluminescence emission bands with peaks at 506 nm and 611 nm, respectively, both in chloroform solution. The long absorption tail ranging into the 600–700 nm region and the large Stokes shift points to a high degree of geometrical disorder in the arrangement of the 9,10-anthrylene chromophores along the distorted polymer backbone. This disorder is borne out in the unusually strong wavelength dependence of fluorescence depolarisation, both with regards to the excitation and the emission wavelengths. Picosecond fluorescence depolarisation spectroscopy provides clear evidence for the presence of orthogonal transition dipole moments, presumably arising from the off-axis transition of the anthracene unit and the on-axis transition of the polymer backbone. Intramolecular energy relaxation then gives rise to the observed fluorescence depolarization dynamics.

Key words conjugated polymers, poly(arylene ethynylene)s, reductive coupling, fluorescence anisotropy

Introduction

Attractive optical and electronic properties of conjugated polymers, in combination with a superior processability, predestine them for many applications, such as in organic field-effect transistors,¹ organic light emitting diodes (OLEDs),^{2–4} photovoltaic devices,⁵ or thin film sensors,⁶ as well as for applications in biology.^{7,8} In this context, poly(arylene ethynylene)s (PAEs) that are composed of alternating arylene and ethynylene units represent one well-established and promising class of conjugated polymers.³ Many PAEs show interesting photoluminescence (PL) properties, in particular stimuli-responsive PL features, together with a high PL efficiency.^{9–13} The two main synthetic routes towards linear PAEs are Sonogashira–Hagihara-type cross-coupling protocols of difunctional monomers containing two ethynyl and halo functions (AA/BB- or AB-type monomers), or alkyne metathesis schemes starting from acyclic, dialkynylarylene monomers.¹⁴

Anthracene is a promising building block for conjugated polymers. Due to its unique features, such as a blueish PL of high quantum yield, it seems well suited for applications in luminescent devices.^{15–18} OLEDs based on anthracene-derived active materials exhibited promising blue electroluminescence properties.^{9,19–21} However, the photooxidation of anthracene under ambient conditions poses a challenge to its usability. Photooxidation can be limited by lowering the reactivity through electron-accepting substituents.²² Therefore, the incorporation of anthracene building blocks into PAEs is particularly interesting.^{9,10,17,23} An intense PL can be expected if stacking of the anthracenes in such a polymer can be prevented.

Nevertheless, soluble poly(9,10-anthrylene ethynylene)s have not been reported previously. The known anthracene-containing PAEs also contain non-anthracene arylene units.⁹ Only insoluble, on-surface synthesized poly(anthrylene ethynylene)s were reported recently.²³

Another interesting property of anthracene single crystals is the high degree of linear polarization of light emission, documented by the fluorescence polarization anisotropy.²⁴ The transition dipole moment is oriented along the short molecular axis of anthracene.^{25–27} Emitters with a macroscopically polarized emission have been investigated for their potential to increase the luminescence efficiency of optical devices. For example, brightness losses caused by polarizers in displays could be reduced, potentially lowering the energy consumption.²⁸ Furthermore, it has been shown that a defined orientation of the emitting dipoles in OLEDs increases the outcoupling efficiency of light out of the device plane, limiting waveguide losses.^{29–31}

Here, we report a novel synthesis scheme of a soluble poly(9,10-anthrylene ethynylene), as a prototypical, direct example for the synthesis of related polymers. Poly[2,6-(2-octyldecyl)-9,10-anthrylene ethynylene] (**PAAE**) was made in the course of the PhD project of one of the co-authors.³² To prevent steric hindrance and distortion of the polymer backbones, and to possibly also suppress the interchain π -stacking of anthrylene units, branched and bulky alkyl side chains were introduced to the outer benzene rings of the anthracenes at the 2,6-positions. Our monomer synthesis is based on published anthracene substitution chemistry.⁹ The optical properties of the **PAAE** polymer obtained were related to commercially available

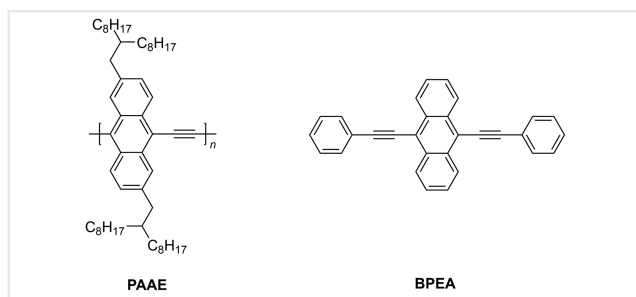
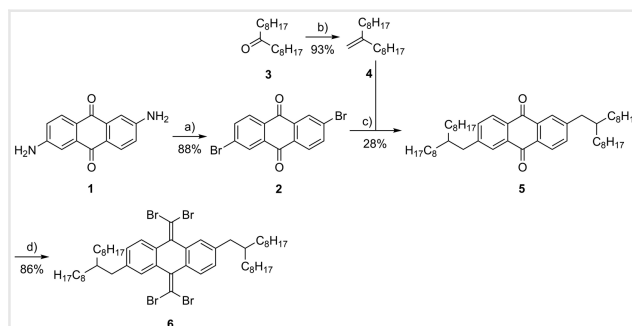


Figure 1 Structure of poly[2,6-(2-octyldecyl)-9,10-anthrylene ethynylene] **PAAE** and the commercially available model compound **BPEA**.

9,10-bis(phenylethynyl)anthracene (**BPEA**) as a monomeric model compound. The chemical structures of the targets are depicted in Figure 1.

Results and Discussion

Our new **PAAE** synthesis is a reductive, dehalogenative homocoupling of 9,10-bis(dibromomethylene)-

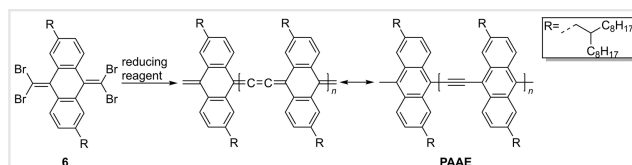


Scheme 1 Synthesis of monomer **6**: a) t -BuNO₂, CuBr₂, ACN, 85 °C, 4 h; b) NaH, Ph₃PMeBr, DMSO, rt, 20 h; c) 1. 9-BBN, THF, rt, 23 h, 2. Pd(PPh₃)₄, K₂CO₃, 75 °C, 23 h; d) CBr₄, Ph₃P, toluene, 80 °C, 24 h.

2,6-bis(2-octyldecyl)-9,10-dihydroanthracene (**6**) as a single monomer. First, the three-step monomer synthesis is depicted in Scheme 1.

Commercially available 2,6-diaminoanthraquinone (**1**) was dibrominated to **2** (88% yield) in a Sandmeyer procedure, as described by Seidel et al.³³ The alkyl side chains were introduced by following a method reported by Müllen's group.⁹ First, 9-heptadecanone (**3**) was converted to 9-methyleneheptadecane (**4**) in a Wittig reaction in 93% yield. The obtained olefin **4** was borylated with 9-borabicyclo[3.3.1]nonane (9-BBN). In a one-pot reaction, the obtained boronic ester was not isolated and immediately coupled with the 2,6-dibromoanthraquinone **2**, leading to the 2,6-dialkylated anthraquinone **5** (28% overall yield). In the last step, a twofold Corey–Fuchs reaction was carried out, as described by Pola et al.³⁴ Under conversion of the keto into dibromomethylene functions, **5** was converted to the desired monomer **6** (86% yield).

Our target poly(anthrylene ethynylene) **PAAE** was synthesized as depicted in Scheme 2. This route is inspired by the on-surface coupling procedure of related non-alkylated monomers as reported by Sánchez-Grande et al.²³ For the resulting polymer, both possible isomeric electron structures are depicted, a cumulene-type and a PAE-type structure, which is expected to be more stable. Both electronic structures, of course, differ in their end groups. It is anticipated that the initially formed olefinic dibromomethylene >CBr_2 end groups (corresponding to the cumulene-type structure) are converted into single-bonded end groups (present for the PAE structure) in an interplay of hydrolysis and water/methanol addition, under



Scheme 2 Synthesis of poly(9,10-anthrylene ethynylene) **PAAE**.

Table 1 Reagent screening for the synthesis of PAEE

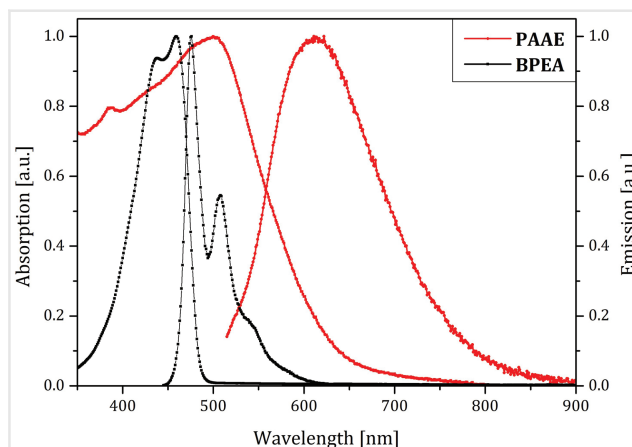
Reagent	Ethyl acetate fraction		Chloroform fraction	
	Yield [%]	Molecular weights M_n/M_w [g/mol]	Yield [%]	Molecular weights M_n/M_w [g/mol]
$\text{Co}_2(\text{CO})_8$	0.4	5500/7300	0.3	5300/8000
$\text{Cr}_2(\text{OAc})_4$, $\text{Ni}(\text{COD})_2$, $\text{Ni}(\text{PPh}_3)(\text{CO})_2$, Cu , Zn , Zn/CuCl	–	–	–	–
<i>n</i> -BuLi, CuCN	53	7100/16600	1	13000/44400

formation of carbonyl-containing end groups (e.g. $-\text{COOH}$, $-\text{COOMe}$, $-\text{CHO}$). In the IR spectrum of **PAEE**, as expected, carbonyl-related signatures at frequencies of 1727 and 1675 cm^{-1} are observed (see Figure S3) that can generally be attributed to carbonyl end groups without the possibility of a clear structural assignment. The Raman spectrum of **PAEE** displays the expected carbon–carbon triple bond stretching vibration at 2161 cm^{-1} (Figure S4).

Different potentially promising reducing reagents have been reported in the literature.^{35–40} The results in terms of the **PAEE** synthesis are summarized in Table 1. Only one of these agents, the combination of *n*-butyllithium (*n*-BuLi) and copper (I) cyanide (CuCN), produced the desired polymer in acceptable yields. The crude products were purified and fractionated by repeated Soxhlet extractions (see the Experimental Section). The molecular weights of the ethyl acetate and chloroform fractions were determined by gel permeation chromatography (GPC, polystyrene calibration). Our method, using *n*-BuLi/CuCN as reagents, yielded 53% **PAEE** with $M_n = 7100$ g/mol and $M_w = 16600$ g/mol (PDI: 2.33, DP: ca. 10) in the ethyl acetate fraction accompanied by a low amount of higher M_n polymer in the chloroform fraction (see Table 1). The good solubility in ethyl acetate is caused by the long-chained, branched alkyl substituents.

A thermogravimetric analysis (TGA) of **PAEE** was carried out in the temperature range from 35 °C to 950 °C with a heating rate of 10 K/min. **PAEE** shows a good thermal stability with a 5% weight loss point at 279 °C. No phase transitions were observed in a differential scanning calorimetry (DSC) analysis in the temperature range from –20 °C to 150 °C (heating rate: 10 K/min).

The absorption and emission spectra of **PAEE** and of the model compound **BPEA** in chloroform solution are displayed in Figure 2. The absorption spectrum of **PAEE** shows a broad absorption band with a peak at 502 nm, arising from the $\pi-\pi^*$ transitions; a similar peak position appears in the thin film at 506 nm. The fact that the optical spectra in solution and the solid state are very similar indicates the absence of interchain interactions. The absorption spectra are surprisingly broad, most probably because of distortion and coiling of the backbone. Indeed, the distortion of neighbouring 9,10-

**Figure 2** Absorption and emission spectra of poly(9,10-anthrylene ethynylene) **PAEE** and the model compound **BPEA** in chloroform solution.

anthrylene units in a related dianthrylacetylene dimer has previously been reported,⁴¹ as has the occurrence of broadened, unstructured absorption bands in related trimers.^{42,43} The bulky alkyl chains at the 2,6-positions of the 9,10-anthrylene units may cause additional disorder. These conclusions are supported by the large Stokes loss associated with the orange/red emission of **PAEE** (peaking at 611 nm in solution, and at 687 nm in the film).

In contrast, the solution absorption spectrum of the monomeric **BPEA** shows the expected narrowed absorption band peaking at 459 nm (film, **BPEA** embedded in a PS matrix: λ_{max} 470 nm). The emission, on the other hand, shifts from 475 nm (solution, shoulders at 508 nm and 536 nm) to a weakly structured, broad band peaking at 568 nm in the film, probably caused by intermolecular interactions in the solid state. Comparing the monomer **BPEA** and the polymer **PAEE**, the overall absorption redshift upon going from the monomer to the polymer is only moderate, suggesting that the overall backbone conjugation is also rather modest. However, polymer formation is also accompanied by a pronounced spectral broadening of the absorption band, presumably as a result of a high degree of geometrical disorder within the polymer backbone. The measured PL quantum yields of the polymer **PAEE** are rather low: 0.072 in solution and 0.038 in films; for comparison, the values for **BPEA** are 0.93 in solution⁴⁰ and 0.19 in films.

By photoemission spectroscopy (see the Experimental Section), the HOMO energy level of **PAEE** was measured as $E_{\text{HOMO}} = -5.49$ eV. Together with an optical bandgap of $E_{\text{g}}^{\text{opt}} = 2.24$ eV (calculated from the absorption onset of the film⁴⁴), the energetic position of the LUMO was estimated to be $E_{\text{LUMO}} = -3.25$ eV.

A particularly interesting aspect regarding the optical properties of the **PAEE** polymer relates to the question of whether signatures of the two transition dipole moments of

the molecule can be resolved. In a simplistic picture, one would expect one axis of polarization to be associated with transitions vertical to the backbone direction, along the axis of the anthracene moieties, and a second polarization component along the arylene ethynylene backbone. Bending of the polymer chain would be expected to limit the overall polarization anisotropy. It is particularly insightful to perform measurements of the loss in polarization memory as a function of time so as to resolve structural dynamics, rotational diffusion, and intramolecular electronic relaxation such as energy transfer from one part of the molecule to another.⁴⁵ Since the excited-state lifetime is dominated by non-radiative relaxation in the polymer, the PL lifetime is smaller than 1 ns. Using a conventional streak-camera system for picosecond polarization-resolved fluorimetry, we define the polarization memory as $r = (I_{\parallel} - GI_{\perp}) / (I_{\parallel} + 2GI_{\perp})$, where I indicates the fluorescence intensity, either parallel or orthogonal to the polarization plane of the excitation laser, and the factor G accounts for the polarization sensitivity of the grating used in the fluorimeter. The measurement setup is sketched in Figure 3. The anisotropy r can be measured either as a function of time, $r(t)$, or as a function of emission wavelength, $r(\lambda_{\text{em}})$. A perfect dipole such as a dye molecule, randomly

distributed in three dimensions, will generally yield an initial anisotropy value of $r(t = 0) = 0.4$,²⁵ which decreases with time because of rotational diffusion. The model monomer structure **BPEA** indeed behaves as such a near-perfect dipole, with $r(t)$ dropping to zero within 250 ps after excitation by a femtosecond laser pulse. As would be expected, we find no linear dichroism in the luminescence, i.e. $r(t)$ is the same over the entire emission spectrum. The situation is very different, and rather unusual, for the polymer **PAAE** as summarized in Figure 3. We begin by discussing $r(t)$ in panel (a). Since the absorption spectrum shown in Figure 2 is so broad, and presumably consists of contributions from both localized anthracene and delocalized **PAAE** chromophores, it is meaningful to alter the excitation wavelength used in the depolarization measurements while detecting the fluorescence in the spectral region of 500–550 nm. When exciting at 490 nm (red curve), $r(t)$ begins at a substantial value of 0.3, dropping down to 0.15 within the measurement window of 2000 ps of approximately three times the fluorescence lifetime. Under this condition, a significant memory of the polarization plane of the incident laser is retained in the fluorescence and we propose that this case corresponds to direct excitation of the polymer backbone. The drop in r with time may arise from structural dynamics such as rotational diffusion, but could also relate to intrachain excited-state energy transfer in the bent polymer structure. As the excitation wavelength λ_{ex} is lowered from 490 nm to 400 nm, a dramatic change takes place, even though the PL spectra remain identical: the initial polarization anisotropy drops continuously with decreasing excitation wavelength, reaching zero within approximately the excited-state lifetime for $\lambda_{\text{ex}} = 400$ nm. Such a complete loss of polarization memory is unusual, even for the most distorted of polymer chains.⁴⁶ We propose that this complete depolarization arises from excited-state relaxation from an excited state of the polymer associated with an off-axis transition-dipole moment along the anthracene unit to the excited state associated with the **PAAE** backbone of the polymer. However, such intramolecular excited-state relaxation would be expected to be very fast and should occur within a few picoseconds. In contrast, a finite but small initial anisotropy of 0.05 is observed, which decays further over time, presumably due to rotation of the molecule in solution. The fact that such rotational diffusion can be observed, even for excitation of the anthracene unit, is consistent with the rather short chain length inferred for the polymer.

It is insightful to examine the spectral dependence of the polarization anisotropy $r(\lambda_{\text{em}})$ as a function of λ_{ex} , shown in Figure 3b. As noted, for a monodisperse system such as a dye molecule, $r(\lambda_{\text{em}})$ shows a constant value over the entire PL spectra which decreases as $r(t)$. However, if different molecular geometries are present in the sample and contribute to the spectral broadening both in the absorption and the emission, signatures of anomalous linear dichroism may arise. Indeed, for all λ_{ex} , we find that $r(\lambda_{\text{em}})$, recorded in the first 300 ps after

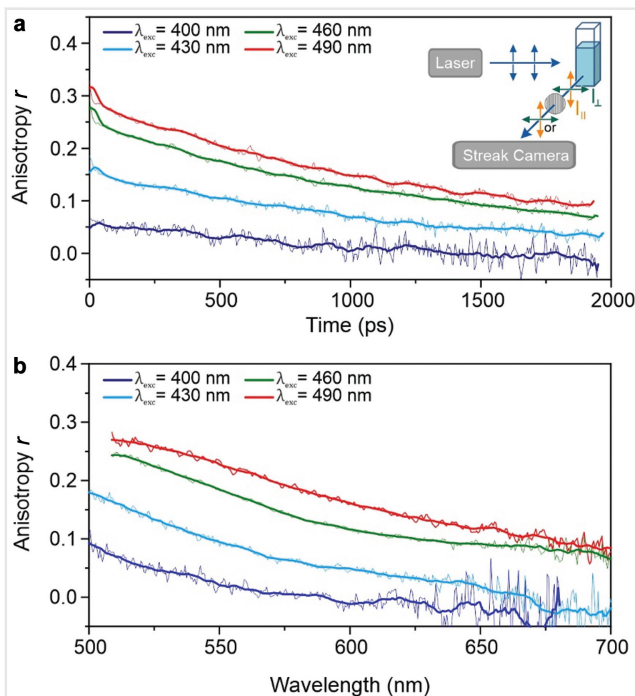


Figure 3 Sketch of the setup to measure the polarization anisotropy in the fluorescence of the polymer **PAAE** in toluene solution using vertically oriented polarization of the excitation laser and detecting either parallel or perpendicular emission polarization components. a) Temporal evolution of the polarization memory for different excitation wavelengths. The fluorescence was detected in a spectral window of 500–550 nm. b) Spectral dependence of the fluorescence depolarization, detected in a time window of 300 ps after photoexcitation.

photoexcitation, decreases with increasing λ_{em} . This unusual observation provides a clear indication of the heterogeneity of the polymer sample, presumably due to the high degree of polydispersity. Emission at longer wavelengths corresponds to longer conjugated segments, which in turn offer more opportunity for the polarization memory to be lost, for example due to distortions in the chain.

The measurement of $r(\lambda_{em})$ therefore offers a spectroscopic route of mapping out the origin of strong spectral broadening of the polymer spectra compared to the monomer. We note that, with a long-pass filter cutting off the luminescence above the maximum around 560 nm, perfectly unpolarized luminescence can be achieved for excitation at 400 nm. While this was not the original objective of our study, this observation appears to be quite unique in the context of the photophysics of conjugated polymers.

Conclusions

A soluble poly(9,10-anthrylene ethynylene), poly[2,6-(2-octyldecyl)-9,10-anthrylene ethynylene] **PAAE**, was made accessible with moderately low degrees of polymerization P_n of ca. 10 in a reductive, dehalogenative homocoupling scheme starting from a 2,6-dialkylated 9,10-bis(dibromomethylene)-9,10-dihydroanthracene monomer. By testing different potential coupling agents, it was found that only the *n*-BuLi/CuCN system allowed for **PAAE** synthesis. **PAAE** shows very broad, unstructured optical spectra, both in absorption and PL, with peak maxima at 506 and 611 nm, respectively, for chloroform solutions. The absorption tails into the 600–700 nm spectral region. Together with the large Stokes loss, these findings indicate a high degree of geometrical disorder of the chromophores that are incorporated into a highly distorted polymer backbone. This conclusion was confirmed by detailed time-resolved studies of the polarization anisotropy in fluorescence. The polarization memory was found to be strongly dependent on excitation wavelength, decreasing with decreasing excitation wavelength, thus providing an indication of orthogonal transition dipole moments within the polymer. In addition, the polarization memory decreases with increasing detection wavelength, which presumably probes molecules of greater extension and thus of greater structural disorder.

Experimental Section

All commercially available chemicals and solvents including dried solvents were obtained from the suppliers Fisher Scientific, Sigma-Aldrich Co., ABCR GmbH, VWR International GmbH, TCI Deutschland GmbH, chemPUR GmbH, Carl Roth GmbH + Co. KG, Santa Cruz Biotechnology Inc. and Merck KGaA, and were used without further purification. Acetoni-

trile was dried over calcium hydride and stored over a molecular sieve (3 Å). Reactions under argon atmosphere were carried out using standard Schlenk techniques and flame-dried glassware. Reactions were monitored by thin-layer chromatography using ALUGRAM® SIL G/UV 254 silica gel plates from Macherey-Nagel with a thickness of 0.2 mm, the TLC plates visualized by UV light at 254 or 365 nm or by common staining reagents. Flash column chromatography was carried out on a Biotage (Isolera One) system with pre-packed silica gel columns from Büchi Labortechnik GmbH. ^1H - and $^{13}\text{C}\{\text{H}\}$ -NMR spectra were recorded on a Bruker AVANCE 400 MHz- or AVANCE III 600 MHz-NMR spectrometers in deuterated solvents. All spectra were referenced to the residual solvent signal. Spin multiplicities were given as follows: s (singlet), d (doublet), t (triplet), q (quartet), m (multiplet), dd (doublet of doublets). FD (field desorption) mass spectra were obtained from a JEOL AccuTOF-GCX spectrometer. GPC measurements were carried out on a PSS/Agilent SECurity GPC system equipped with a diode array detector (G1362A) and a refractive index detector (G1362A). Separation was carried out on a set of two PSS SDV Linear S columns (8 × 300 mm, particle size 5 μm) and a PSS SDV precolumn (8 × 300 mm, particle size 5 μm) at room temperature, using chloroform or THF as the eluents (flow rate: 1 mL/min) and polystyrene standards. UV/Vis absorption spectra were recorded on a Jasco V-670 spectrometer. The IR spectrum was prepared with a Jasco FT/IR 4700 spectrometer using an ATR unit. The Raman spectrum of a thin film of the polymer was measured with a confocal Raman microscope (MonoVista CRS+ from S&I), with 633 nm as the excitation wavelength. Thin films (thickness: 20 nm) were prepared by spin coating a polymer solution in chloroform (4 mg/mL) on a silicon substrate. To increase the Raman signal compared to the strong PL of the polymer, approximately 1 nm of silver was deposited by thermal evaporation on top of the polymer film. As a reference the same silver layer was also deposited on the pristine Si substrate. PL spectra were measured on a Horiba Scientific FluoroMax-4 spectrometer at room temperature. Quantum yields were obtained with an integrating sphere accessory (QuantaPhi). Spin-coated polymer films were obtained from 7 mg/mL solutions on quartz glass using a Süß MicroTec spin-coater (rotational speed: 1000 rpm). HOMO energy levels were determined by atmospheric pressure photoelectron spectroscopy on a Riken Keiki (AC-2) spectrometer. TGA and DSC were carried out with a Mettler Toledo TGA/DSC1 STAR-System under an argon stream of 50 mL/min and a heating rate of 10 K/min.

Picosecond fluorescence depolarization was measured using a frequency-doubled tunable femtosecond Ti:sapphire laser (Coherent, Chameleon Ultra II) for excitation and a streak camera (Hamamatsu c5680 series) coupled to a spectrometer (Brucker, 250is c68878) for detection. The analyte was dissolved in toluene solution and further diluted to rule out reabsorption effects during the measurements.

2,6-Dibromoanthraquinone 2

To a refluxing mixture of *tert*-butyl nitrite (8.4 mL, 63.6 mmol, 3.0 equiv), copper (II) bromide (11.91 g, 53.3 mmol, 2.5 equiv) and dry acetonitrile (350 mL) under an argon atmosphere, 2,6-diaminoanthraquinone **1** (5.0 g, 21.0 mmol, 1.0 equiv) was slowly added. After 4 hours the mixture was cooled to room temperature and poured into a 1 M aqueous hydrochloric acid solution. The crude, precipitated 2,6-dibromobromo-9,10-anthraquinone **2** was filtered off and the product purified by recrystallization from chloroform. The product was obtained as a light-yellow solid (6.74 g, 18.43 mmol, 88%).

¹H-NMR (600 MHz, CDCl₃, 323 K): δ [ppm] = 8.44 (2 H, d, J = 2.0 Hz), 8.17 (2 H, d, J = 8.3 Hz), 7.94 (2 H, dd, J = 8.3, 2.0 Hz). **¹³C-NMR** (151 MHz, CDCl₃, 323 K): δ [ppm] = 181.4, 137.5, 134.7, 132.2, 130.6, 130.4, 129.3. **MS** (FD): m/z = 363.8816, calculated for [C₁₄H₆O₂Br₂]⁺ = 363.8735.

9-Methyleneheptadecane 4

60% Sodium hydride in mineral oil (0.79 g, 19.7 mmol, 1.0 equiv) was added to dry dimethyl sulfoxide (8 mL) under an argon atmosphere and heated to 75 °C for 20 minutes. Then, the mixture was cooled to 0 °C and triphenylmethylphosphonium bromide (7.02 g, 19.7 mmol, 1.0 equiv) in warm dimethyl sulfoxide (20 mL) was added. The resulting solution was stirred for 10 minutes at room temperature. Subsequently, 9-heptadecanone **3** (5.00 g, 19.7 mmol, 1.0 equiv) was added and the mixture stirred for 20 hours. Then, saturated aqueous ammonium chloride solution was added under cooling. The solution was extracted with pentane, dried over magnesium sulphate and evaporated. The crude product was purified by column chromatography (hexane) to yield product **4** as a colourless liquid (4.60 g, 18.2 mmol, 93%).

¹H-NMR (400 MHz, CDCl₃, 300 K): δ [ppm] = 4.69 (2 H, s), 2.00 (4 H, t, J = 7.6 Hz), 1.48–1.20 (24 H, m), 0.89 (6 H, t, J = 6.9 Hz). **¹³C-NMR** (101 MHz, CDCl₃, 300 K): δ [ppm] = 150.6, 108.5, 36.3, 32.1, 29.7, 29.6, 29.5, 28.0, 22.9, 14.3. **MS** (FD): m/z = 252.2931, calculated for [C₁₈H₃₆]⁺ = 252.2817.

2,6-Bis(2-octyldecyl)anthraquinone 5

A 0.5 M 9-borabicyclo[3.3.1]nonane solution in THF (62 mL, 31.0 mmol, 2.7 equiv) was slowly added to 9-methyleneheptadecane **4** (7.13 g, 28.2 mmol, 2.5 equiv) under an argon atmosphere at room temperature. The mixture was stirred for 23 hours. Then, a 2.4 M aqueous potassium carbonate solution (10 mL, 23.5 mmol, 2.1 equiv), 2,6-dibromoanthraquinone **2** (4.14 g, 11.3 mmol, 1.0 equiv) and tetrakis(triphenylphosphino)palladium (0) (0.52 g, 0.45 mmol, 0.04 equiv) were added. The mixture was heated

to 75 °C for a further 23 hours. Then, the reaction mixture was cooled down to room temperature, extracted with dichloromethane, dried over magnesium sulphate, and evaporated to dryness. The crude product was purified by column chromatography (eluent: hexane/CH₂Cl₂ 1/0 to 3/1). The product **5** was obtained as yellow oil (2.24 g, 3.14 mmol, 28%).

¹H-NMR (600 MHz, CDCl₃, 300 K): δ [ppm] = 8.21 (2 H, d, J = 7.9 Hz), 8.07 (2 H, d, J = 1.5 Hz), 7.55 (2 H, dd, J = 7.9, 1.7 Hz), 2.70 (4 H, d, J = 7.1 Hz), 1.72 (2 H, s), 1.37–1.15 (58H, m), 0.86 (12 H, t, J = 7.0 Hz). **¹³C-NMR** (151 MHz, CDCl₃, 300 K): δ [ppm] = 183.6, 149.6, 135.0, 133.6, 131.7, 127.7, 127.4, 41.1, 39.8, 33.4, 32.0, 30.1, 29.7, 29.5, 26.7, 22.8, 14.2. **MS** (FD): m/z = 712.6186, calculated for [C₅₀H₈₀O₂]⁺ = 712.6158.

9,10-Bis(dibromomethylene)-2,6-bis(2-octyldecyl)-9,10-dihydroanthracene 6

Dry toluene (5 mL) was added to triphenylphosphine (2.31 g, 8.79 mmol, 8.0 equiv) and tetrabromomethane (1.64 g, 4.95 mmol, 4.5 equiv) under an argon atmosphere. The mixture was stirred for 20 minutes at room temperature. Then, 2,6-bis(2-octyldecyl)-9,10-anthraquinone **6** (0.78 g, 1.10 mmol, 1.0 equiv) in toluene (5 mL) was added and the mixture was heated to 80 °C for 24 hours. The suspension was cooled down to room temperature and filtered. The isolated solid was washed with toluene and the filtrate evaporated to dryness. The crude products were purified by column chromatography (eluent: hexane). Monomer **6** was obtained as colourless oil (0.97, 0.95 mmol, 86%).

¹H-NMR (600 MHz, CDCl₃, 300 K): δ [ppm] = 7.73 (2 H, d, J = 8.0 Hz), 7.60 (2 H, d, J = 1.5 Hz), 7.04 (2 H, dd, J = 8.0, 1.7 Hz), 2.52 (4 H, d, J = 6.8), 1.63 (2 H, m), 1.34–1.17 (58H, m), 0.88 (12H, t, J = 7.1 Hz). **¹³C-NMR** (151 MHz, CDCl₃, 300 K): δ [ppm] = 141.1, 139.9, 135.9, 133.3, 128.4, 127.9, 127.4, 89.4, 40.6, 39.8, 33.5, 33.2, 32.1, 30.2, 30.1, 29.8, 29.7, 29.5, 29.4, 27.1, 26.9, 26.6, 22.8, 14.3. **MS** (FD): m/z = 1020.2935, calculated for [C₅₀H₈₀Br₄]⁺ = 1020.2994.

Poly[2,6-(2-octyldecyl)-9,10-anthrylene ethynylene] PAEE

A solution of the monomer 9,10-bis(dibromomethylene)-2,6-bis(2-octyldecyl)-9,10-dihydroanthracene **6** (1.34 g, 1.31 mmol, 1.0 equiv) in dry tetrahydrofuran (10 mL) was cooled to temperatures below –90 °C. Then, 1.6 M *n*-BuLi solution in hexane (1.64 mL, 2.62 mmol, 2.0 equiv) was slowly added. The solution was stirred for 1 hour. Subsequently, copper(I) cyanide (0.12 g, 1.31 mmol, 1.0 equiv) was added and the mixture allowed to slowly reach room temperature, over a period of c. 4 hours. The mixture was further stirred at room temperature for 18 hours. Then, the

mixture was diluted with chloroform and washed twice with 25% aqueous ammonia solution. In the organic phase, most of the solvent was evaporated. The polymer was subsequently precipitated into acidified (2 M HCl) cold methanol, isolated by filtration, and washed with methanol. The crude product was purified by subsequent Soxhlet extractions (MeOH, acetone, EtOAc, CHCl₃). **PAAE** was obtained as a dark red, viscous mass (ethyl acetate fraction: 0.49 g, 0.70 mmol, 53%; chloroform fraction: 0.01 g, 0.01 mmol, 1%).

¹H-NMR (400 MHz, C₂D₂Cl₄, 353 K): δ [ppm] = 9.21–6.48 (m), 3.15–2.22 (m), 2.14–1.78 (m), 1.78–1.00 (m), 1.00–0.17 (m). **GPC** (THF) ethyl acetate fraction: M_n = 7100, M_w = 16600 g/mol; chloroform fraction: M_n = 13000, M_w = 44400 g/mol. **UV/Vis** CHCl₃ solution: λ_{max} [nm] = 261, 502; film: λ_{max} [nm] = 263, 506. **PL** CHCl₃ solution (λ_{exc} [nm] = 500 nm): λ_{max} [nm] = 611, PL quantum yield [PLQY] = 7.2%; film (λ_{exc} [nm] = 500 nm): λ_{max} [nm] = 687, PLQY = 3.8%. **HOMO/LUMO energies**: E_{HOMO} [eV] = –5.49; E_{LUMO} [eV] = –3.25; E_g [eV] = 2.24.

Supporting Information

Supporting Information for this article is available online at <https://doi.org/10.1055/a-1472-6806>.

References

- (1) Kim, M.; Ryu, S. U.; Park, S. A.; Choi, K.; Kim, T.; Chung, D.; Park, T. *Adv. Funct. Mater.* **2019**, *10*, 1904545.
- (2) So, F.; Krummacker, B.; Mathai, M. K.; Poplavskyy, D.; Choulis, S. A.; Choong, V.-E. *J. Appl. Phys.* **2007**, *102*, 91101.
- (3) Ragni, R.; Operamolla, A.; Farinola, G. M. Synthesis of Electroluminescent Conjugated Polymers for OLEDs. In *Organic Light-Emitting Diodes (OLEDs)*; Buckley, A., Ed.; Cambridge UK: Elsevier; **2013**, 3–48.
- (4) Burroughes, J. H.; Bradley, D. D. C.; Brown, A. R.; Marks, R. N.; Mackay, K.; Friend, R. H.; Burns, P. L.; Holmes, A. B. *Nature* **1990**, *347*, 539.
- (5) Günes, S.; Neugebauer, H.; Sariciftci, N. S. *Chem. Rev.* **2007**, *107*, 1324.
- (6) Zhou, H.; Chua, M. H.; Tang, B. Z.; Xu, J. *Polym. Chem.* **2019**, *10*, 3822.
- (7) Wang, Y.; Feng, L.; Wang, S. *Adv. Funct. Mater.* **2019**, *29*, 1806818.
- (8) Baek, P.; Voorhaar, L.; Barker, D.; Travas-Sejdic, J. *Acc. Chem. Res.* **2018**, *51*, 1581.
- (9) Yang, C.; Jacob, J.; Müllen, K. *Macromol. Chem. Phys.* **2006**, *207*, 1107.
- (10) Bunz, U. H. F. *Macromol. Rapid Commun.* **2009**, *30*, 772.
- (11) Jiang, D.-L.; Choi, C.-K.; Honda, K.; Li, W.-S.; Yuzawa, T.; Aida, T. *J. Am. Chem. Soc.* **2004**, *126*, 12084.
- (12) Lee, K.; Cho, J. C.; Deheck, J.; Kim, J. *Chem. Commun.* **2006**, *18*, 1983.
- (13) Zhao, X.; Pinto, M. R.; Hardison, L. M.; Mwaura, J.; Müller, J.; Jiang, H.; Witker, D.; Kleiman, V. D.; Reynolds, J. R.; Schanze, K. S. *Macromolecules* **2006**, *39*, 6355.
- (14) Bunz, U. H. F. *Chem. Rev.* **2000**, *100*, 1605.
- (15) Tarkuç, S.; Eelkema, R.; Grozema, F. C. *Tetrahedron* **2017**, *73*, 4994.
- (16) Parada, G. A.; Goldsmith, Z. K.; Kolmar, S.; Pettersson Rimgard, B.; Mercado, B. Q.; Hammarström, L.; Hammes-Schiffer, S.; Mayer, J. M. *Science* **2019**, *364*, 471.
- (17) Eaton, D. F. *Pure Appl. Chem.* **1988**, *60*, 1107.
- (18) Vorona, M. Y.; Yutronkie, N. J.; Melville, O. A.; Daszczyński, A. J.; Agyei, K. T.; Ovens, J. S.; Brusso, J. L.; Lessard, B. H. *Materials* **2019**, *12*, 2726.
- (19) Wen, H.-Y.; Huang, T.-S.; Zhang, H.-D.; Chang, M.-Y.; Huang, W.-Y. *ACS Appl. Polym. Mater.* **2019**, *1*, 3343.
- (20) Halder, S.; Chakraborty, D.; Roy, B.; Banappanavar, G.; Rinku, K.; Mullangi, D.; Hazra, P.; Kabra, D.; Vaidhyathan, R. J. *Am. Chem. Soc.* **2018**, *140*, 13367.
- (21) Shih, H.-M.; Lin, C.-J.; Tseng, S.-R.; Lin, C.-H.; Hsu, C.-S. *Macromol. Chem. Phys.* **2011**, *212*, 1100.
- (22) Tember, T. M.; Cherkasov, A. S. *Theor. Exp. Chem.* **1973**, *7*, 332.
- (23) Sánchez-Grande, A.; de La Torre, B.; Santos, J.; Cirera, B.; Lauwaet, K.; Chutora, T.; Edalatmanesh, S.; Mutombo, P.; Rosen, J.; Zbořil, R.; Miranda, R.; Bjork, J.; Jelinek, P.; Martin, N.; Eciya, D. *Angew. Chem. Int. Ed.* **2019**, *58*, 6559.
- (24) Ganguly, S. C.; Choudhury, N. K. *Z. Phys.* **1953**, *135*, 255.
- (25) Lakowicz, J. R. *Principles of Fluorescence Spectroscopy*. Springer: Boston, **2006**.
- (26) Uejima, M.; Sato, T.; Tanaka, K.; Kaji, H. *Chem. Phys.* **2014**, *430*, 47.
- (27) Choudhury, N. K. *Z. Phys.* **1958**, *151*, 93.
- (28) Men, J.; Ting, H.; Li, Y.; Wang, W.; Gao, G.; Xiao, L.; Chen, Z.; Wang, S.; Gong, Q. *Chem. Phys. Lett.* **2014**, *609*, 33.
- (29) Senes, A.; Meskers, S. C. J.; Dijkstra, W. M.; van Franeker, J. J.; Altazin, S.; Wilson, J. S.; Janssen, R. A. J. *J. Mater. Chem. C* **2016**, *4*, 6302.
- (30) Frischeisen, J.; Yokoyama, D.; Endo, A.; Adachi, C.; Brütting, W. *Org. Electron.* **2011**, *12*, 809.
- (31) Miteva, T.; Meisel, A.; Grell, M.; Nothofer, H. G.; Lupo, D.; Yasuda, A.; Knoll, W.; Kloppenburg, L.; Bunz, U. H. F.; Scherf, U.; Neher, D. *Synth. Met.* **2000**, *111–112*, 173.
- (32) Geisler, I. S. Dissertation. Bergische Universität Wuppertal: Germany, **2020**.
- (33) Seidel, N.; Hahn, T.; Liebing, S.; Seichter, W.; Kortus, J.; Weber, E. *New J. Chem.* **2013**, *37*, 601.
- (34) Pola, S.; Kuo, C.-H.; Peng, W.-T.; Islam, M. M.; Chao, I.; Tao, Y.-T. *Chem. Mater.* **2012**, *24*, 2566.
- (35) Baysec, S.; Preis, E.; Allard, S.; Scherf, U. *Macromol. Rapid Commun.* **2016**, *37*, 1802.
- (36) Hörhold, H.-H.; Gottschaldt, J.; Opfermann, J. *J. Prakt. Chem.* **1977**, *319*, 611.
- (37) Reisch, H.; Wiesler, U.; Scherf, U.; Tuytuykov, N. *Macromolecules* **1996**, *29*, 8204.
- (38) Buckles, R. E.; Matlack, G. M. *Org. Synth., Coll.* **1963**, *4*, 914; *Org. Synth.* **1951**, *31*, 104.
- (39) Rawson, R. J.; Harrison, I. T. *J. Org. Chem.* **1970**, *35*, 2057.
- (40) Iyoda, M.; Otani, H.; Oda, M. *Angew. Chem.* **1988**, *100*, 1131.
- (41) Nishioka, T.; Kuroda, K.; Akita, M.; Yoshizawa, M. *Angew. Chem. Int. Ed. Engl.* **2019**, *58*, 6579.
- (42) Dell'Aquila, A.; Marinelli, F.; Tey, J.; Keg, P.; Lam, Y.-M.; Kapitanchuk, O. L.; Mastroianni, P.; Nobile, C. F.; Cosma, P.; Marchenko, A.; Fichou, D.; Mhaisalkar, S. G.; Suranna, G. P.; Torsi, L. *J. Mater. Chem.* **2008**, *18*, 786.
- (43) Keg, P.; Dell'Aquila, A.; Marinelli, F.; Kapitanchuk, O. L.; Fichou, D.; Mastroianni, P.; Romanazzi, G.; Suranna, G. P.; Torsi, L.; Lam, Y.-M.; Mhaisalkar, S. G. *J. Mater. Chem.* **2010**, *20*, 2448.
- (44) Souharce, B. Dissertation. Bergische Universität Wuppertal: Germany, **2008**.
- (45) Thiessen, A.; Würsch, D.; Jester, S. S.; Aggarwal, A. V.; Idelson, A.; Bange, S.; Vogelsang, J.; Höger, S.; Lupton, J. M. *J. Phys. Chem. B* **2015**, *119*, 9949.
- (46) Ruseckas, A.; Wood, P.; Samuel, I. D. W.; Webster, G. R.; Mitchell, W. J.; Burn, P. L.; Sundström, V. *Phys. Rev. B: Condens. Matter* **2005**, *72*, 115214.